Article

Chinese Science Bulletin

Oceanology

October 2012 Vol.57 No.30: 3908–3916
doi: 10.1007/s11434-012-5234-8

A quasi-global 1/10° eddy-resolving ocean general circulation model and its preliminary results

YU YongQiang*, LIU HaiLong & LIN PengFei

State Key Laboratory of Atmospheric Sciences and Geophysical Fluid Dynamics, Institute of Atmospheric Physics, Chinese Academy of Sciences, Beijing 100029, China

Received January 8, 2012; accepted March 2, 2012; published online June 17, 2012

In this study, a quasi-global (excluding the Arctic Ocean) eddy-resolving ocean general circulation model (OGCM) is established based on the latest version of the LASG/IAP Climate system Ocean Model (LICOM2.0). The horizontal resolution and vertical resolution are increased to 1/10° and 55 layers, respectively. Forced by the surface fluxes from the reanalysis and observed data, the model has been integrated for approximately 20 model years (20 a). During the last 8 a, the model is driven by daily mean wind stresses from QuikSCAT and heat fluxes from reanalysis data from 2000 to 2007. The basic performance of the OGCM is analyzed using the last 8 a simulation output. Compared with the simulation of the coarse-resolution OGCM, the eddy-resolving OGCM not only better simulates the spatial-temporal features of mesoscale eddies and the paths and positions of western boundary currents but also reproduces the large meander of the Kuroshio Current and its interannual variability. Another aspect, namely, the complex structures of equatorial Pacific currents and currents in the coastal ocean of China, are better captured due to the increased horizontal and vertical resolution.

ocean general circulation model (OGCM), mesoscale eddy, eddy-resolving, western boundary currents

Citation: Yu Y Q, Liu H L, Lin P F. A quasi-global 1/10° eddy-resolving ocean general circulation model and its preliminary results. Chin Sci Bull, 2012, 57: 3908–3916, doi: 10.1007/s11434-012-5234-8

The first baroclinic Rossby radius of deformation in the ocean is at least one order of magnitude smaller than that in the atmosphere due to the differences in density, compressibility and other physical features between the ocean and atmosphere, although both atmospheric and oceanic motions are governed by similar geophysical fluid dynamics equations. The spatial scale of synoptic eddies in the atmosphere is approximately 1000 km, while the corresponding spatial scale of synoptic eddies is approximately 50–200 km in the ocean. These eddies are called oceanic mesoscale eddies. Studies have shown that oceanic mesoscale eddies are a basic form of oceanic motions. Because the kinetic energy of mesoscale eddies is at least 3–4 times that of mean circulations, they play an important role in the energy cycle. As an important form of motion, these eddies not only intimately interact with large-scale circulations but also affect and modulate the evolution of oceanic ecosystems.

To simulate the features and climatic effects of mesoscale eddies, the horizontal resolution of the Oceanic General Circulation Model (OGCM) must be at least 1/10° or finer. Only when the mesoscale eddies are directly resolved in ocean models can their basic features be captured. Generally, an OGCM with horizontal grid less than 1/10° is called an eddy-resolving OGCM. Because of its high horizontal resolution, both the complex topography at the sea floor and the land-sea distribution are better captured in an eddy-resolving OGCM. The spatiotemporal features of western boundary currents and other narrow currents are also better reproduced in eddy-resolving models. Thus, the development and application of eddy-resolving OGCMs are given increasingly more attention for studies of physical oceanology and climate.

Due to the limits of computer resources, only a few studies on the numerical simulation of mesoscale eddies using

*Corresponding author (email: yyq@lasg.iap.ac.cn)

global OGCMs have been published thus far. Since the late 1990s, many studies have focused on the simulation of mesoscale eddies in the North Atlantic basin [1–3]. With the development and increase of computer capabilities, several researchers have simulated mesoscale eddies using global eddy-resolving OGCMs [4–8]. Table 1 shows eddy-resolving simulations performed with the most popular OGCMs in the world. Their results indicate that the kinetic energies of mesoscale eddies are closer to those derived from satellite altimeters in eddy-resolving OGCMs compared with simulations from coarse-resolution OGCMs. Meanwhile, the strengths and paths of the western boundary currents and their extensions are better captured.

Given the importance of OGCMs in the atmosphere and ocean sciences, the scientists at LASG/IAP have been devoting themselves to independently developing a global OGCM since the late 1980s. Zhang et al. [9] developed the first OGCM in China. This OGCM has a horizontal resolution of 4°×5° and has 4 layers in the vertical. The physical processes and spatial resolutions have since been improved by the LASG/IAP scientists. Until now, four generations of OGCMs have been developed [9–12]. These OGCMs have been coupled with different atmospheric GCMs, and the simulations have been joined in the Coupled Model Intercomparison Project (CMIP). The fourth-generation OGCM is called the LASG/IAP Climate system Ocean Model (LICOM), which has two versions: LICOM1.0 and LICOM2.0. The details of LICOM2.0 can be found in [13]. Based on the LICOM2.0, we construct an eddy-resolving OGCM by increasing the horizontal grids from 1° to 1/10° globally and changing some dynamical frame and parallel schemes, after which, a simulation using eddy-resolving LICOM is achieved.

1 OGCM and experiment design

Based on the LICOM2.0 [13], we build a quasi-global eddy-resolving eddy OGCM. The updates and improvements include the following. (1) The horizontal grids are increased to 1/10°. (2) The vertical layers are increased to 55 layers. The thickness of the first layer is 5 m. The upper 300 m has 36 uneven layers, and the mean thickness is less than 10 m. (3) The model domain is from 66°N–79°S, and thus, the Arctic Ocean is excluded. (4) Biharmonic viscosity and diffusivity schemes are used at the horizontal directions in the equations of momentums and tracers (temperature and salinity), respectively. Meanwhile, the parameterization of mesoscale eddies from Gent and McWilliams [14] is turned off in the equations of tracers. (5) The barotropic and baroclinic split methods are improved. (6) The parallel domain partition is changed froma one-dimensional (1D) Message Passing Interface (MPI) meridionalsplit to a mixed two-dimensional (2D) MPI and Open MP. The Open MP parallel algorithm is optimized.

The eddy-resolving OGCM is forced by the climatologically monthly wind stress and heat fluxes and is initialized by the observed temperature and salinity, which is the spin-up integration. The eddy-resolving OGCM is integrated for 12 years from zero velocity. The forcing data are from Ocean Model Intercomparison Project (OMIP) [15], which is derived from ERA15 reanalysis data [16]. In addition, the simulated sea surface salinity (SSS) is restored to the climatologically monthly SSS from Levitus data [17]. Because the northern open boundary is set at 66°N, the simulated temperature and salinity are restored to the climatologically monthly temperature and salinity from the Levitus data [17], while the solid wall boundary condition is used for velocity.

After the 12-year spin-up numerical simulations, the eddy-resolving OGCM is integrated an additional 8-year starting from the end of the 12th year spin-up simulation. The model is forced by the daily QuickSCAT wind stress [18] during the 2000–2007 period and surface heat and freshwater fluxes derived from COREs [19] during this period. The detailed algorithm to calculate the turbulent surface fluxes can be found in [19]. Because the sea ice model is not included in LICOM2.0, the sea ice concentration is used from the Hadley dataset [20] to calculate the surface fluxes. Because the temperature of the seawater is below the freezing point (−1.8°C), the temperature is restored to −1.8°C. The last 8-year simulations are used for analysis in the present study.

2 Results

2.1 Mesoscale eddies and western boundary currents

The basic features of large-scale ocean circulations are well simulated in the coarse-resolution LICOM2.0 [13]. The climatologically mean large-scale ocean circulations in the eddy-resolving LICOM are similar to those in the coarse-resolution LICOM, such as subtropical gyres in the Atlantic

Table 1 Brief introduction of studies on the numerical simulations of eddy-resolving[a)]

Models	POP	NLOM	MOM	POP	MOM	NLOM	HYCOM	NLOM
Domain	Atlantic	Atlantic	Atlantic	Global	Global	Global	Global	Global
Integration time	16 a	*n*/a	4 a	15 a	55 a	*n*/a	17 a	*n*/a
Horizontal grid (°)	1/10	1/16	1/12	1/10	1/10	1/16	1/25	1/32
Reference	[1]	[2]	[3]	[4]	[5]	[6]	[7]	[8]

a) NLCOM is a reduced-gravity model for operational forecasting and was not integrated for a long period of time.

and Pacific, subpolar gyres and the Antarctic Circumpolar Current (ACC). However, the transient sea surface height (SSH) in the eddy-resolving LICOM shows numerous mesoscale eddies, particularly along the Kuroshio Current and its extension, the Gulf Stream and its extension and areas around the ACC. The mesoscale eddies in these regions are the most active. The standard deviation (STD) of the SSH can clearly reflect the statistical features of mesoscale eddies. Figure 1 shows the STD of the SSHA from satellite altimeter, eddy-resolving and coarse-resolution OGCMs. The altimeter SSH is the weekly Maps of Sea Level Anomalies (MSLA) during 2000–2007, with a horizontal resolution of 1/4° [21]. Compared with the coarse-resolution OGCM, the eddy-resolving OGCM reproduces a more realistic distribution and strength (STD magnitude) of SSHA. For example, a large STD is located around the western boundary currents and their extensions and around the ACC. In addition, a relatively large STD exists in the subtropical countercurrents in the northwest Pacific between 20° and 30°N. In general, the STD in the eddy-resolving OGCMs is larger than that of the observation in most regions. For the coarse-resolution OGCM, the STD is one-third less than that in the observation or an eddy-resolving OGCM because the coarse-resolution OGCM cannot resolve mesoscale eddies. This characteristic implies that the kinetic energy in a coarse-resolution OGCM must be much smaller than that in the observations and an eddy-resolving OGCM.

At the horizontal plane, mesoscale eddies reflect cyclonic or anti-cyclonic quasi-geostrophic motions, which are associated with strong vertical motions (ascending or descending) due to the friction effect. Therefore, the temperature structures can also reflect the features of mesoscale eddies. Figure 2 shows the transient 50-m temperature fields on January 1, 2007, in four major western boundary current regions simulated by eddy-resolving LICOM. The features of the Kuroshio, the Gulf Stream, the East Australia current, the Agulus current and their extensions are well captured. Their spatial widths are all approximately 100 km, and the separation positions are generally consistent with the observed results. Meanwhile, there are large errors in the widths of the western boundary currents and the spilt-positions of the extensions simulated by the coarse-resolution OGCM due to the larger grid distance (e.g. the coarse-resolution LICOM with a horizontal resolution of 1° and the extensions of the Kuroshio and the Gulf Stream separating from the western boundary currents at approximately 39°N). The separation position is located 2°–3° farther north of the observed, which will induce errors in the simulated temperatures, salinities and currents. These errors are common issues, and they exist in other coarse-resolution OGCMs. Meanwhile, the eddy-resolving LICOM can simulate the mesoscale eddies around the western boundary currents and their extensions, which are represented by the cold and warm centers with a horizontal scale of approximately several hundred kilometers, corresponding to cyclonic or anti-cyclonic circulations, respectively. This feature cannot be well simulated by the coarse OGCMs (not shown).

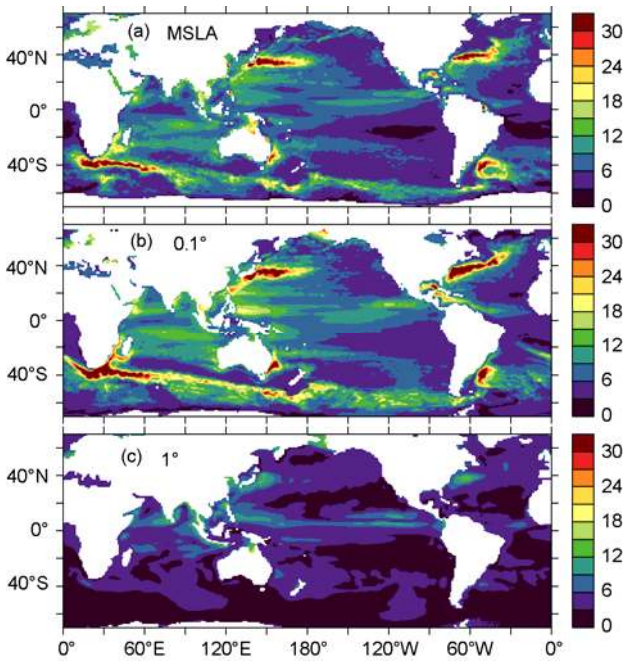

Figure 1 The STD of weekly SSHA (cm) from a satellite altimeter during 2000-01-02–2007-12-19 (MSLA), eddy-resolving LICOM (1/10°) and coarse-resolution LICOM (1°) during 2000-01-01–2007-12-31. The daily SSHA is also used in the coarse-resolution OGCM.

The Kuroshio, located in the northwest Pacific, is one of the most important western boundary currents, and it can affect the climate and environment of China to a large extent. The Kuroshio axis or path has significant interannual variability, particularly in the appearance of an obviously large, twisting path south of Japan in some years. This feature is called the large meander of Kuroshio. The physical mechanism of the large meander is complex and remains unclear [22]. Figure 3 shows the yearly mean Kuroshio path during 2000–2007 simulated by the eddy-resolving LICOM. The Kuroshio path is denoted by 14°C isotherm lines at approximately 300 m. Obviously, the interannual variability of the simulated Kuroshio path is strongly associated with the appearance of a large meander south of Japan in some years. The largest meander appears in 2005, while the straightestpath appears in 2007. Figure 4(a) and (b) shows the yearly mean SSHA from the satellite altimeter, which reflects the sea surface circulation anomalies. In 2005, a negative SSHA is dominant south of Japan, while in 2007, a positive SSHA is located south of Japan. The negative and positive SSHAs correspond to the large meander in 2005 and the straight path in 2007, respectively. The yearly mean SSHA distributions are basically simulated as the observed distributions in 2005 and 2007 (Figure 4(c) and (d)). Between 135°–140°E and 30°–34°N, southeast of Japan, there is an obvious negative SSHA in 2005 and a positive

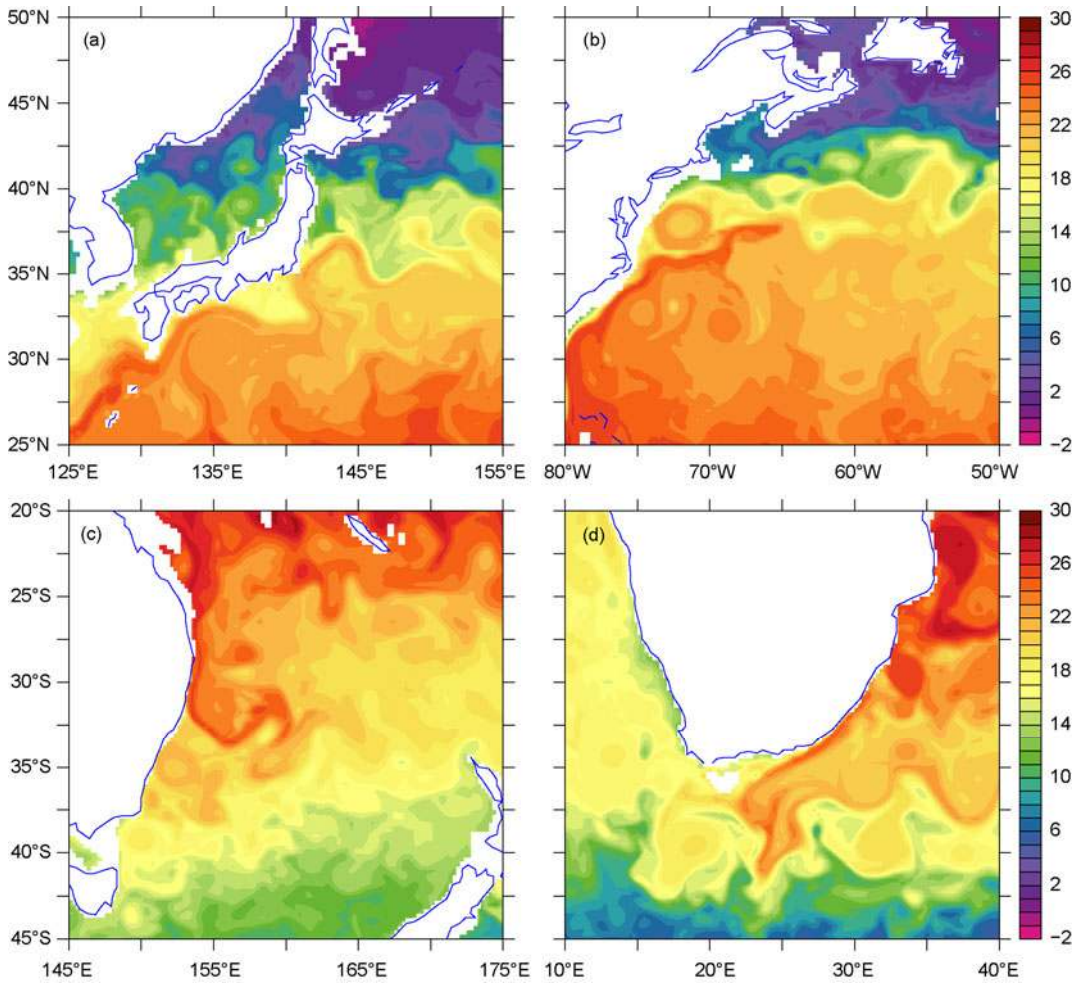

Figure 2 The transient 50 m temperature (°C) fields on 2007-01-01 in four major western boundary currents regions simulated by eddy-resolving LICOM. (a) Kuroshio; (b) Gulf Stream; (c) East Australian Current; (d) Agulhas Current.

SSHA in 2007 in the eddy-resolving LICOM, corresponding to those observed. It should be noted that the simulated Kuroshio meanders and the corresponding mesoscale eddies are more evident than those observed, which are shown in Figures 3 and 4. The physical mechanism of these strong signals is left for future study and analysis. Aside from the Kuroshio meander south of Japan, the Kuroshio axis shows a relatively stable meander change at approximately 144°E and 150°E, which is consistent with the observed [22].

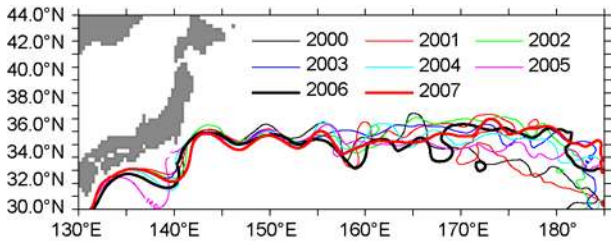

Figure 3 Yearly mean 14°C isotherm lines of approximately 300 m during 2000–2007 simulated by the eddy-resolving LICOM. The isotherm lines denote the Kuroshio axis. Different colors represent different years.

Some studies have noted that the meanders in these two locations are related to the topographical forcing. Others have found that the meanders are due to the interaction between mean current and mesoscale eddies.

2.2 Oceanic circulation in the tropical Pacific

With an increase in the model's horizontal and vertical resolution, the eddy-resolving model realistically simulates the complex structure of currents in the upper tropical ocean. For example, the depth-latitude section along 155°W clearly exhibits the South Equatorial Current (SEC), North Equatorial Current (NEC) and North Equatorial Counter Current (NECC) at the surface and the Equatorial Undercurrent (EUC), South Surface Counter Current (SSCC), North Surface Counter Current (SSCC), and Equatorial Intermediate Current (EIC) below the surface (Figure 5). The locations of these currents are very similar to those from the observation [23], although three (EIC, NSCC and SSCC) are weaker. For the section along 165°E, the model shows similar results, but it fails to simulate the NECC. In contrast, in the

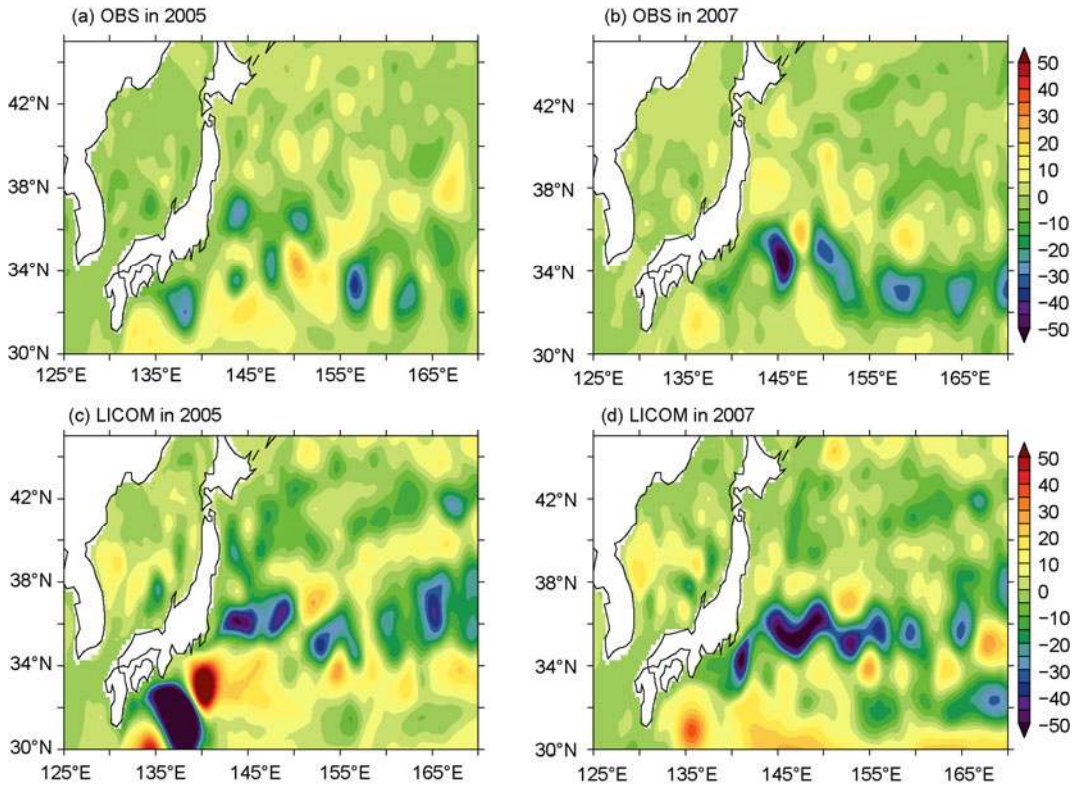

Figure 4 The yearly mean SSHA (cm) from the satellite altimeter in 2005 (a) and 2007 (b); (c) and (d) are the same as in (a) and (b) for the simulated SSHA by the eddy-resolving LICOM.

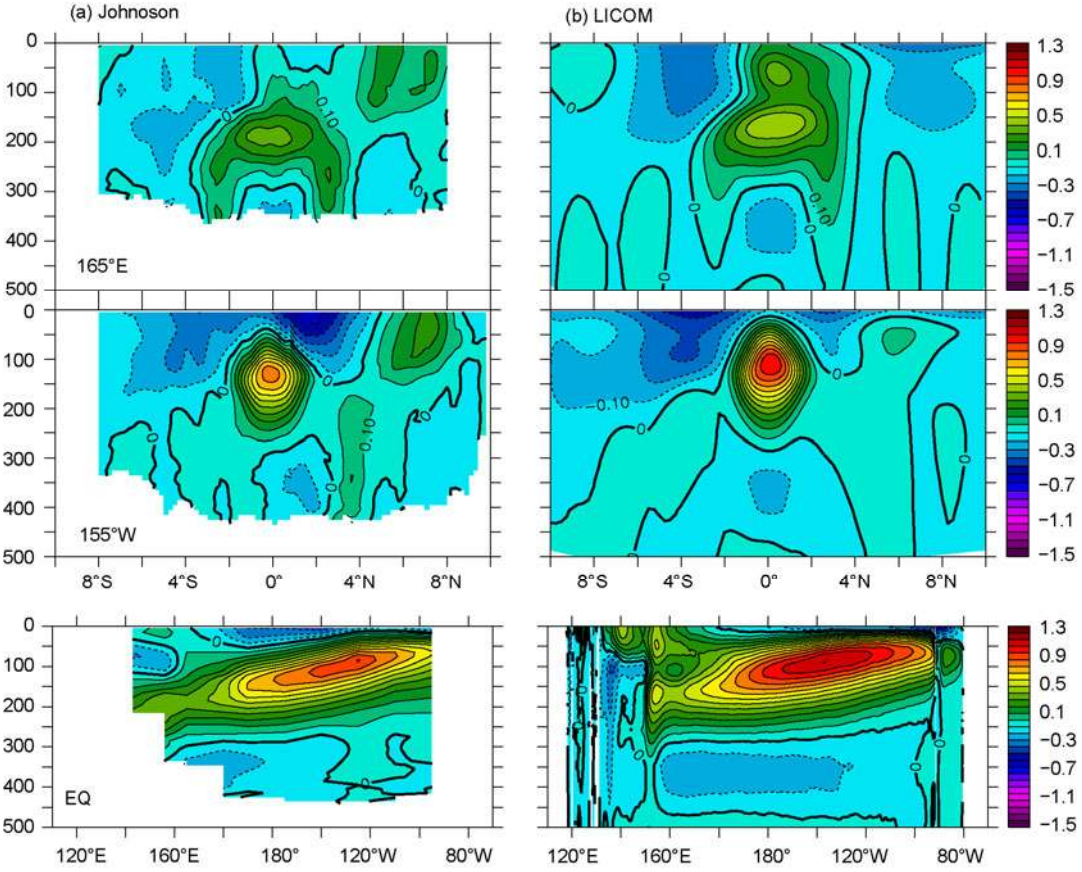

Figure 5 Zonal current along 165°E (upper), 155°W (middle) and the equator (lower) for observation (a) that is plotted based on [23] and on model (b) in the tropical Pacific (unit: m/s).

latitude-depth sections along 155°W or 165°E, even the longitude-depth section averaged between 1°S and 1°N, the simulated EUC is much stronger than the observed by approximately 15%, and the simulated vertical extension of the EUC is also larger than the observed. These numerical experiments demonstrated that the strength of the EUC is highly sensitive to horizontal viscosity, e.g. the reduced horizontal viscosity could significantly strengthen EUC [11]. The coarse resolution (1° for horizontal resolution) of the LICOM2.0 only simulated the SEC, NEC, NECC and EUC in the upper thermocline (not shown here), which is similar to other simulations with coarse resolution. However, the eddy-resolving version of LICOM2.0 can reproduce the SSCC, NSCC, and EIC with realistic location and strength, which implies that the spatial resolution is the key ingredient for successfully simulating baroclinic structure in the upper ocean. In addition, when the resolution is increased, the model can better simulate the basic features of the tropical instability wave (TIW) (not shown here).

2.3 Marginal seas near China

A series of marginal seas is located in the western Pacific from south to north and mainly include the South China Sea (SCS), the East China Sea, the Yellow Sea, and the Sea of Japan. Thus, in the strict sense, the western boundary cannot be regarded as a solid wall in the Northwest Pacific because there is a close relationship between the oceanic circulations in the marginal seas and the western boundary current. On one hand, a branch of the Kuroshio can enter into Yellow Sea (called the Yellow Sea Warm Current) [24]; on the other hand, the water exchanges between the Kuroshio and South China Sea are extremely complex, e.g. a water mass can invade South China through a circulation loop or countercyclonic eddy-shedding from the Kuroshio and can sometimes flow northward directly without any exchange [25–28]. Because the description of the coastline and topography in the eddy-resolving model has been significantly improved, the model should better reproduce the principal features of circulation in marginal seas near China. To evaluate the model's ability to simulate the circulations in the marginal sea, Figure 6 shows the temperatures and currents at 50 m for February and August in the marginal seas near China, which are divided into two subregions—the SCS, and other marginal seas—from which an overview of the coastal ocean circulation of China in the summer and winter can be inferred.

The main body of the Kuroshio flows northeast along the Okinawa Trough and turns eastward after reaching southern Japan. The simulated SST for February shows that a warm tongue lies in the central Yellow Sea andthe Tsushima Strait, and a northward current prevails at the surface (Figure 6 (upper panel)), which implies that a small portion of the Kuroshio water may cross through the continental shelf. This so-called Yellow Sea Warm Current (YSWC) and the Tsushima Warm Current have been explored by many observational studies. It is necessary to note that the simulated YSWC is not located in the center of the basin but is slightly west of the center, which is consistent with the observational and theoretical studies [29,30]. Meanwhile, a warm zone is located northeast of Taiwan Island that extends northward to the Yangtze River Estuary, which reflects the impact of the Taiwan warm current. The sea temperature is lower than 10°C at 50 m in the Yellow Sea in August, in obvious contrast to the warm water of the Kuroshio. This lower sea temperature is the observed Yellow Sea Cold Water Mass.

In the South China Sea, the surface current driven by the dominant northeast winter monsoon in February mainly shows a basin-scale cyclonic circulation (Figure 6 (lower panel)). The Kuroshio water invades the SCS by the way of a loop, i.e. it enters south of the Luzon Strait and exits north of the Luzon Strait. In August, however, the summer southwest monsoon prevails in the SCS, an the surface circulation is characterized by double gyres, of which the cyclonic gyre is dominant in the north basin and the anticyclonic gyre is dominant in the south basin. In contrast to the pathway of the Kuroshio in February, the main body of the Kuroshio travels northward directly rather than enteringthe SCS. The mass transport through the Luzon Strait is also greatly weakened in August. Further diagnosis demonstrates that the simulated volume transport across the Luzon Strait is −7.97, −0.18, −0.47, and −5.97 Sv for January, April, July, and October (the negative value represents transport from the Pacific to the SCS), respectively. Therefore, there is a net volume transport into the South China Sea for each calendar season, and the annual mean is −3.67 Sv. The estimated transport is consistent with many other observational and modeling studies. For example, Chu et al. [31] suggested that the net transport estimated from the P-vector method is −13.47 Sv in winter and −1.4 Sv in summer, and the transport estimated from the different models varies from −5 to −20 Sv in winter and −1.6 to −3.1 Sv in summer [32–35]. Generally speaking, the simulated volume transport through Luzon Strait in this paper is comparable with that reported by most studies.

In addition, if we analyze the time evolution of the daily mean sea surface temperature or sea surface height outputted from the model, in addition to the Kuroshio loop invading the South China Sea, we can find eddy shedding from the Kuroshio into the SCS at any time of the year (not shown here), which is basically consistent with the findings in [27,28]. However, the mesoscale eddies generated in the SCS are different from those shed from the Kuroshioas suggested by [28]. Therefore, we need further and comprehensive evaluations of the models to reproduce the mesoscale eddies in the South China Sea.

One of challenging tasks in simulating the SCS circulation is its warm current, which is a countercurrent in the northeast of the SCS in winter. This current originates from

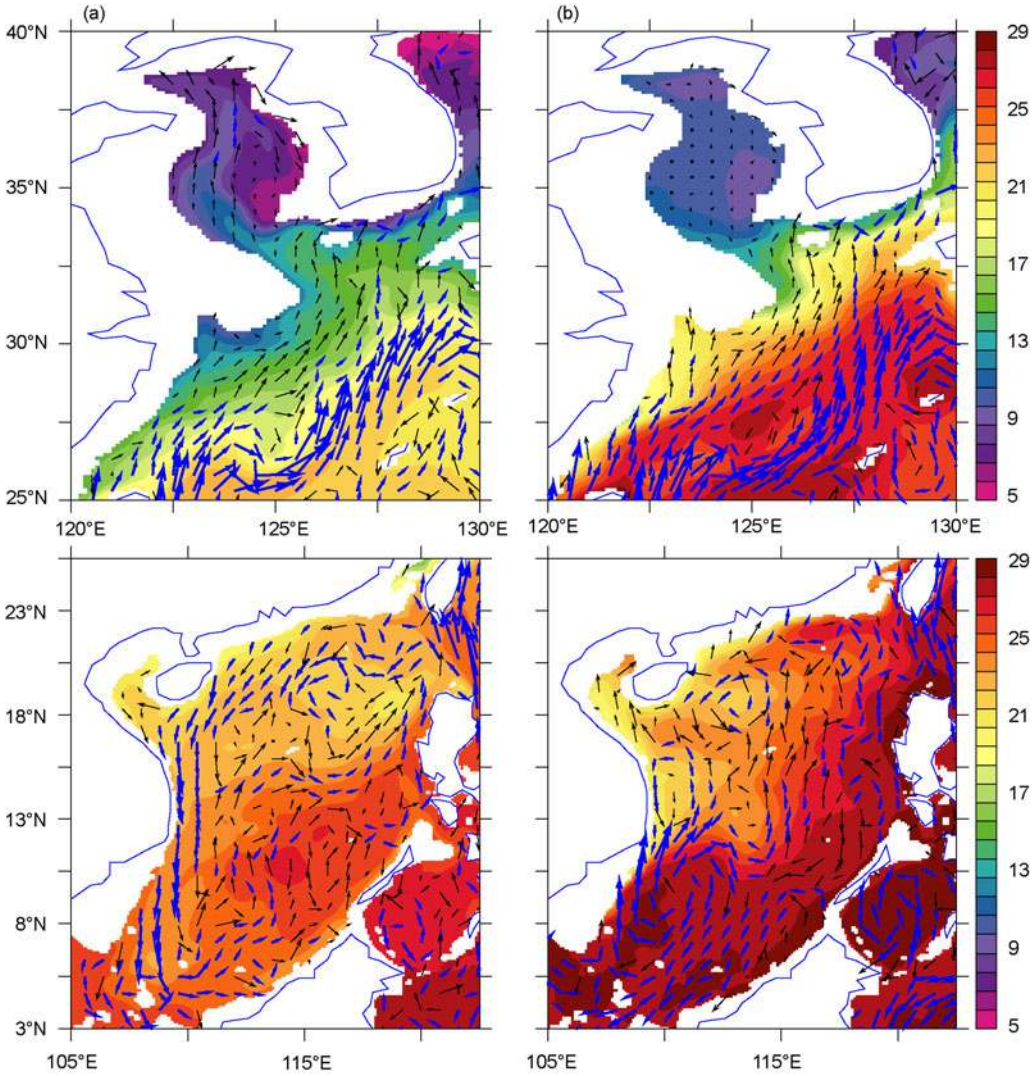

Figure 6 Simulated temperature (shaded) and current (vector) at 50 m for February (a) and August (b). Unit: °C and m/s, blue (black) arrows denote a velocity greater (lesser) than 0.1 m/s.

Hainan Island and passes through the Taiwan Strait along the shelf and finally entersthe East China Sea [36]. After analyzing the simulated surface current at 10 m in winter, we find that LICOM can simulate the countercurrent through the Taiwan Strait but fails to simulate the countercurrent along the shelf in the east of Hainan Island (not shown). Based on the previous study [37], we suggest that this failure may be related to the bias in the spatial structure of the density over the shelf of the north SCS.

3 Summary and discussion

Based on the global oceanic general circulation model LICOM2.0, after improving the physical parameterization schemes, dynamic framework, and paralleling algorithms, we establish a quasi-global (excluding the Arctic Ocean) eddy-resolving model with a 1/10° resolution and 55 layers in the vertical; the model was integrated for 20 model years. The present study analyzes the model output in the last 8 model years and preliminarily evaluates the simulated large-scale circulations, mesoscale eddies and China's coastal ocean circulations. The principal conclusions are as follows:

(1) The model well reproduces the observed characteristics of the energy of mesoscale eddies. The spatial pattern of the standard deviation of the sea surface height reproduced by the model is close to the observed spatial pattern and is much better than the corresponding coarse-resolution model, in which the active regions with mesoscale eddies are mainly located near the western boundary currents, the Antarctic Circumpolar Circulation (ACC) and the Subtropical Counter Currents (STCC).

(2) The model well simulates the magnitude and path of the western boundary currents and the location where the western boundary currents separate from the boundaries. In particular, the large meander of the Kuroshio can be simu-

lated in the model, along with its transition from a straight path to a meandering path. Further diagnosis shows a close relationship between the Kuroshio and coastal circulations. For example, the Taiwan warm current, the Yellow Sea Warm Current, the invasion of the Kuroshio into the South China Sea, and the Yellow Sea Cold Water Mass are successfully simulated in the model.

(3) With the help of the increased spatial resolution, the vertical structure of the equatorial currents is better reproduced in the model than that in its previous versions. Although the Equatorial Undercurrent (EUC) is overestimated, the eddy-resolving model can simulate the Equatorial Intermediate Current (EIC), the South Surface Counter Current (SSCC) and the North Surface Counter Current (NSCC).

Compared with the coarse-resolution version of the ocean model LICOM, the performance of the model is significantly improved after its horizontal resolution is increased to 1/10°, but some prominent model biases also exist. For example, the equatorial undercurrent is overestimated and is too shallow, and the north equatorial counter current is greatly underestimated. After comparing wind stress data from QuickSCAT and NCEP reanalyses, Wu et al. [38] found that trade winds from the former are stronger and that the ITCZ is located farther southward than that from the latter, while the former can make the ocean model simulate a stronger equatorial undercurrent and weaker north equatorial countercurrent. In addition, some studies have suggested that the strength of equatorial current system is highly sensitive to horizontal viscosity coefficients [11]. Thus, it is necessary to perform numerical experiments using the eddy-resolving model that further explore the sensitivity of the different branches of the equatorial current system to the vertical and horizontal viscosity and diffusion coefficients in the model along with the relationships among these different currents and corresponding physical mechanisms.

In the present study, we only increased the horizontal and vertical resolutions of model, while the vertical mixing parameterization schemes remained unchanged, as in the coarse-resolution model, and thus, there was no obvious improvement in the simulated mixed layer depth (not shown). In fact, increased resolution and improved physical parameterization schemes are both important. For example, wave-induced mixing is important for improving the mixed layer [39]. Therefore, based on the eddy-resolving model, we will improve the vertical mixing schemes in the model, including wave-induced mixing, tidal mixing, internal wave mixing and the mixing scheme at the bottom boundary, in the future.

This work was supported by the National Basic Research Program of China (2010CB950502), and the Strategic Priority Research Program — Climate Change: Carbon Budget and Related Issues of the Chinese Academy of Sciences (XDA05110302), the National High-tech R&D Program of China (2010AA012304) and China National Science Foundation Committee (40975065 and 41023002). We would like to thank Pu Ye and Dr. Liu Li for their help with the parallelization of the LICOM codes. We also thank Zhang Xuehong for his long-term attention and valuable advice from the beginning to end of the project. The authors are grateful to the Academician Hu Dunxin from the Institute of Oceanography of the Chinese Academy of Sciences and to Profs. Liu Qinyu and Wu Lixin of the Ocean University of China for their suggestions regarding the model assessment and evaluation. We thank three anonymous reviewers for their valuable comments. The first and second 10-year numerical experiments of the ocean model in the present study were completed at the supercomputing center of the Chinese Academy of Sciences and the National Supercomputing Center in Tianjin, respectively.

1 Smith R D, Maltrud M E, Bryan F, et al. Numerical simulation of the North Atlantic Ocean at 1/10°. J Phys Oceanogr, 2000, 30: 1532–1561
2 Hurlburt H E, Hogan P J. Impact of 1/8 degrees to 1/64 degrees resolution on gulf stream model—Data comparisons in basin-scale subtropical Atlantic ocean models. Dyn Atmos Oceans, 2000, 32: 283–329
3 Oschlies A. Improved representation of upper-ocean dynamics and mixed layer depths in a model of the North Atlantic on switching from eddy-permitting to eddy-resolving grid resolution. J Phys Oceanogr, 2002, 32: 2277–2298
4 Maltrud M, McClean J L. An eddy resolving global 1/10 ocean simulation. Ocean Model, 2005, 8: 31–54
5 Masumoto Y, Sasaki H, Kagimoto T, et al. A fifty-year eddy-resolving simulation of the world ocean—Preliminary outcomes of OFES (OGCM for the Earth Simulator). J Earth Simulator, 2004, 1: 35–56
6 Smedstad O M, Hurlburt H E, Metzger E J, et al. An operational eddy resolving 1/16 degrees global ocean nowcast/forecast system. J Mar Syst, 2003, 40: 341–361
7 Thoppil P G, Richman J G, Hogan P J. Energetics of a global ocean circulation model compared to observations. Geophys Res Lett, 2011, 38, doi:10.1029/2011GL048347
8 Shriver J F, Hurlburt H E, Smedstad O M, et al. 1/32° real-time global ocean prediction and value-added over 1/16° resolution. J Mar Syst, 2007, 65: 3–26
9 Zhang X H, Liang X. A numerical world ocean general circulation model. Adv Atmos Sci, 1989, 6: 43–61
10 Zhang X H, Chen K M, Jin X Z, et al. Simulation of thermohaline circulation with a twenty-layer oceanic general circulation model. Theore Appl Clim, 1996, 55: 65–87
11 Jin X Z, Zhang X H, Zhou T J. Fundamental framework and experiments of the third generation of IAP/LASG world ocean general circulation model. Adv Atmos Sci, 1999, 16: 197–215
12 Liu H L, Yu Y Q, Li W, et al. Manual for LASG/IAP Climate System Ocean Model (LICOM1.0) (in Chinese). Beijing: Science Press, 2004. 1–128
13 Liu H L, Lin P F, Yu Y Q, et al. The baseline evaluation of LASG/IAP Climate system Ocean Model (LICOM) version 2.0. Acta Meteorol Sin, 2012, doi: 10.1007/s13351-012-0305-y
14 Gent P R, McWilliams J C. Isopycnal mixing in ocean circulation models. J Phys Oceanogr, 1990, 20: 150–155
15 Röske F. An atlas of surface fluxes based on the ECMWF re-analysis —A climatological dataset to force global ocean general circulation models. Germany, Hamburg MPI: Report No. 323, 2001, 31
16 Gibson J K, Coauthor. ERA Description, ECMWF Reanalysis Project Report Series 1, European Center for Medium Range Weather Forecast. UK: Reading, 1997. 66
17 Levitus S, Boyer T P. World Ocean Atlas 1994: Volume 4: Temperature. NOAA Atlas NESDIS4, U.S. Department of Commerce, Washington DC, 1994. 117
18 CERSAT-IFREMER. QuikSCAT Scatterometer Mean Wind Field Product. User Manual, C2-MUT-W-03-IF, 2002. 48
19 Large W, Yeager S. Diurnal to Decadal Global Forcing for ocean and Sea-Ice Models: The Data Sets and Flux Climatologies, NCAR/TN-460+STR, 2004. 105
20 Rayner N A, Brohan P, Parker D E, et al. Improved analyses of

changes and uncertainties in sea surface temperature measured *in situ* since the mid-nineteenth century: The HadSST2 data set. J Clim, 2006, 19: 446–469
21 Fu L L, Christensen E J, Yamarone C, et al. TOPEX/Poseidon mission overview. J Geophys Res, 1994, 99: 24369–24381
22 Kawabe M. Varaitions of current path, velocity, and volume transport of the Kuroshio in relation with larger meander. J Phys Oceanogr, 1995, 25: 3103–3117
23 Johnson G C, Sloyan B M, Kessler W S, et al. Direct measurements of upper ocean currents and water properties across the tropical Pacific Ocean during the 1990s. Prog Oceanogr, 2002, 52: 31–61
24 Le K T, Mao H L. Wintertime structures of temperature and salinity of the southern Huanghai (Yellow) Sea and its current systems. Oceanol Limnol Sin, 1990, 22: 13–23
25 Li L, Wu B Y. Kuroshio's loop in the South China Sea. Taiwan Strait, 1989, 8: 89–95
26 Nitani H. Beginning of the Kuroshio. In: Stommel H, Yoshida K, eds. Kuroshio. Physical Aspects of the Japan Current. Seattle: University of Washington Press, 1972. 129–163
27 Zhuang W, Xie S P, Wang D, et al. Intraseasonal variability in sea surfaceheight over the South China Sea. J Geophys Res, 2010, 115: C04010
28 Wang D, Xu H, Lin J, et al. Anticyclonic eddies in the northeastern South China Sea during winter 2003/2004. J Oceanogr, 2008, 64: 925–935
29 Lin X, Yang J, Guo J, et al. An asymmetric upwind flow, Yellow Sea Warm Current: 1. New observations in the western Yellow Sea. J Geophys Res, 2011, 116: C04026
30 Lin X, Yang J. An asymmetric upwind flow, Yellow Sea Warm Current: 2. Arrested topographic waves in response to the northwesterly wind. J Geophys Res, 2011, 116: C04027
31 Chu P C, Li R. South China Sea isopycnal-surface circulation. J Phys Oceanogr, 2000, 30: 2419–2438
32 Zhao W, Hou Y J, Le K T, et al. Numerical study on seasonal variation of water exchange in the Luzon Strait. Oceanol Limnol Sin, 2007, 38: 495–503
33 Tian J W, Yang Q X, Liang X F, et al. Observation of Luzon Strait transport, Geophys Res Lett, 2006, 33: L19607
34 Fang G H, Wei Z X, Choi B H, et al. Interbasin freshwater, heat and salt transport through the boundaries of the East and South China Seas from a variable-grid global ocean circulation model. Sci China Ser D: Earth Sci, 2003, 46: 149–161
35 Cai, S Q, Liu H L, Li W, et al. Application of LICOM to the numerical study of the water exchange between the South China Sea and its adjacent oceans. Acta Oceanol Sin, 2005, 24: 10–19
36 Guan B X. Evidence for a counter-wind current in winter off the southeast coast of China. Chin J Oceanol Limnol, 1986, 4: 319– 332
37 Wang D, Hong B, Gan J, et al. Numerical investigation on propulsion of the counter-wind current in the northern South China Sea in winter. Deep-Sea Res I, 2010, 57: 1206–1221
38 Wu F H, Lin P F, Liu H L. Influence of a southern shift of the ITCZ in quick scatterometer on the Pacific North Equatorial Countercurrent. Adv Atmos Sci, 2012, doi: 10.1007/s00376-012-1149-1
39 Qiao F, Yuan Y, Yang Y, et al. Wave-induced mixing in the upper ocean: Distribution and application to a global ocean circulation model. Geophys Res Lett, 2004, 31: L11303